Journal of Nuclear Medicine, published on November 16, 2017 as doi:10.2967/jnumed.117.196279

Characterization of site-specifically conjugated monomethyl auristatin E- and duocarmycin-based anti-PSMA antibody-drug conjugates for treatment of PSMA-expressing tumors

Susanne Lütje[1,2], Danny Gerrits[1], Janneke D. Molkenboer-Kuenen[1], Ken Herrmann[2], Giulio Fracasso[3], Marco Colombatti[3], Otto C. Boerman[1], Sandra Heskamp[1]

[1] Department of Radiology and Nuclear Medicine, Radboud university medical center, Nijmegen, the Netherlands

[2] Clinic for Nuclear Medicine, University Hospital Essen, Germany

[3] Department of Medicine, University of Verona, Verona, Italy

Corresponding author:

Susanne Lütje, MD PhD

Department of Radiology and Nuclear Medicine

Radboud university medical center

Geert Groote Plein 10

6525 GA Nijmegen

The Netherlands

Email: Susanne.Lutje@radboudumc.nl

Phone: 0031 24 36 55340

ABSTRACT

Rationale:

Prostate cancer (PCa) is the most common cancer in men worldwide. In general, PCa responds poorly to chemotherapy. Therefore, antibody-drug conjugates (ADCs) have been developed to specifically deliver highly cytotoxic drugs to the tumor. As the prostate-specific membrane antigen (PSMA) is overexpressed in PCa, it represents a promising target for ADC-based therapies. The aim of this study was to evaluate the therapeutic efficacy of site-specifically conjugated duocarmycin- and monomethyl auristatin E (MMAE)-based anti-PSMA ADCs with drug-antibody ratios (DARs) of 2 and 4.

Methods:

The glycan group of the anti-PSMA antibody D2B was chemoenzymatically conjugated with duocarmycin or MMAE. Preservation of the immunoreactivity of the antibody upon site-specific conjugation was investigated in vitro. Biodistribution and microSPECT/CT imaging (18.5 ± 2.6 MBq) with 25 µg of ^{111}In-labeled ADCs were performed in BALB/c nude mice with s.c. PSMA^{+} LS174T-PSMA xenografts. Finally, the therapeutic efficacy of the four different ADCs was assessed in mice with LS174T-PSMA tumors.

Results:

The immunoreactivity of the anti-PSMA antibody was preserved upon site-specific conjugation. Biodistribution revealed high tumor uptake of all agents, highest tumor uptake was observed in mice administered with ^{111}In-DTPA-D2B-DAR2-MMAE, reaching 119.7 ± 37.4 %ID/g at 3 days p.i. Tumors of mice injected with ^{111}In-DTPA-D2B, ^{111}In-DTPA-D2B-DAR2-duocarmycin, ^{111}In-DTPA-D2B-DAR4-duocarmycin, ^{111}In-DTPA-D2B-DAR2-MMAE, and ^{111}In-DTPA-D2B-DAR4-MMAE could clearly be visualized with microSPECT/CT. In contrast to unconjugated D2B or vehicle, treatment with either MMAE-based ADC, but not with a duocarmycin-based ADC, significantly impaired the tumor growth and prolonged

median survival from 13 days (PBS) to 20 and 29 days for DAR2 and DAR4 ADC, respectively. Tumor doubling time increased from 3.5 ± 0.5 days to 5.2 ± 1.8 and 9.2 ± 2.1 days after treatment with D2B-DAR2-MMAE and D2B-DAR4-MMAE, respectively.

Conclusion:

The site-specifically conjugated anti-PSMA ADCs D2B-DAR2-MMAE and D2B-DAR4-MMAE efficiently targeted PSMA-expressing xenografts, effectively inhibited tumor growth of PSMA-expressing tumors, and significantly prolonged survival of mice.

Key words:

Prostate cancer, prostate-specific membrane antigen (PSMA), antibody-drug conjugate, duocarmycin, monomethyl auristatin E (MMAE)

INTRODUCTION

Prostate cancer (PCa) is the most common cancer in men worldwide leading to substantial morbidity and mortality (*1*). Despite improvements in conventional therapies such as radical prostatectomy with or without radiotherapy, recurrence of the disease frequently occurs. While recurrent disease can temporarily be managed with androgen ablation, PCa can progress to a hormone refractory state, which frequently is accompanied by rapid progression of the disease (*2*). Hormone-refractory PCa usually is difficult to treat and treatment may include chemotherapeutic agents. Unfortunately, chemosensitivity of PCa is limited and responses are weak and accompanied by severe side effects (*3*).

In the past decade, therapy with monoclonal antibodies (mAbs) has attracted a tremendous amount of attention. However, most mAbs show limited anti-tumor activity in unmodified form. To overcome these limitations, mAbs can be covalently bound to cytotoxic drugs to form an antibody-drug conjugate (ADC) which selectively delivers the drug to tumor tissue while reducing toxicity to healthy tissues. In previous studies, it has been shown that the effectiveness of chemotherapeutic agents can be enhanced by conjugation to targeting molecules (*4,5*). Two main categories of cytotoxic drugs are used in ADC development: microtubule inhibitors and DNA-damaging drugs. At present, a variety of ADCs are available for clinical use, such as Kadcyla® (ado-trastuzumab emtansine), an ADC consisting of the anti-HER2 directed mAb trastuzumab and the cytotoxic agent DM1 or Adcetris® (brentuximab vedotin), an ADC containing monomethyl auristatin E (MMAE), is a synthetic dolastatin 10 analogue causing cytotoxicity by inhibition of tubulin polymerization (*6*) and the antibody brentuximab directed against CD30, which is overexpressed in Hodgkin's lymphoma and other T-cell lymphomas.

In PCa, the prostate-specific membrane antigen (PSMA), a type II transmembrane glycoprotein, is abundantly and specifically expressed on PCa cells and internalized upon binding, which renders it an ideal target for ADCs. PSMA has also been found to be expressed in the tumor-associated neovasculature of multiple solid tumor types; therefore PSMA-targeted therapies might not be restricted to PCa but

could also be applied to other malignancies in future (*7-9*). So far, several anti-PSMA-based ADCs have been characterized. Ma et al. reported potent anti-tumor activity of an anti-PSMA mAb conjugated MMAE and report a potent anti-tumor effect in mice with PSMA-positive C4-2 xenografts (*5*). Kuroda and colleagues conjugated the anti-PSMA mAb hJ591 to the ribosome-inactivating protein toxin saporin and reported high anti-tumor activity in an LNCaP xenograft model (*10*), while the same antibody serves as scaffold for the ultra-potent DNA-crosslinking PBD-dimer (ADCT401/MEDI3726), which most recently entered clinical trials (NCT02991911). An ADC consisting of the antibody MLN591, directed against PSMA and the same maytansinoid drug as in Kadcyla® has been evaluated in patients with PCa in a phase I/II clinical trial (*11*). While this study provided proof-of-principle evidence supporting anti-PSMA ADCs as potentially effective agents for patients with PCa, this particular ADC showed limited therapeutic efficacy and possessed an extremely narrow therapeutic window with rapid deconjugation of the drug from the antibody causing dose-dependent peripheral neuropathy (*11*). Two other ADCs targeting PSMA are currently undergoing clinical evaluation, including one containing the same linker technology and payload as present in Adcetris® which has completed phase II and another ADC (ADCT401/MEDI3726) most recently entered clinical trials based on antibody J591 and an ultra-potent DNA-crosslinking PBD-dimer.

Frequently, ADCs are based on random conjugation to naturally available amino acid side chains (ε-amino group of lysines or thiol group of cysteines) which results in stochastic distribution of drug-antibody ratio (DAR), leading to heterogeneous products containing a stochastic mixture of ADCs with different molar DARs and linked at different sites to the antibody. As a consequence, each component in the mixture may have different pharmacokinetics, immunoreactivity, charge, size, and stability (*12*). Random conjugation was shown to reduce the efficacy of ADCs resulting in a low therapeutic index (amount of a therapeutic agent that causes the therapeutic effect in relation to the amount that causes toxicity) in which efficacious and maximum tolerated dose are similar (*13*). An important strategy to

enhance the therapeutic index of a given mAb-drug combination is site-specific conjugation. One of the methods to achieve this is by engineering of a specific amino acid into an antibody which serves as an anchor for attachment of the drug (*12,14*). In the present study, site-specifically conjugated ADCs using the antibody's glycan at asparagine-297 as an anchor were used (*12*). Major advantage of this method is its applicability to any type of recombinant IgG isotype, irrespective of mammalian expression system, and any linker−payload combination (*12*). ADCs produced by this method were found to be homogeneous and highly hydrolytically stable, while displaying negligible aggregation (*12*).

The murine mAb D2B specifically targets PSMA and has been shown to efficiently accumulate in PSMA-expressing LNCaP xenografts (*15*).

The aim of this study was to compare the therapeutic efficacy of four different anti-PSMA ADCs. For this purpose, the mAb D2B was site-specifically conjugated with the cytotoxic drugs MMAE, an irreversible inhibitor of microtubuli, or duocarmycin, a DNA-alkylating agent acting by binding to the minor groove of DNA in A-T rich regions (*16*). To evaluate the relationship between DAR and ADC efficacy, two DAR variants were compared for both anti-PSMA ADCs, one with a DAR of 2 and one with a DAR of 4.

MATERIALS AND METHODS

Preparation of the antibody

The anti-PSMA monoclonal antibody D2B (IgG1) was prepared as described before (*17*). Briefly, it was purified from hybridoma culture supernatant by Protein A affinity chromatography. The antibody secreting cells were obtained according to the hybridoma technology from mice that were immunized with a cell lysate of membranes of LNCaP PCa cells.

Preparation of acid cleavable glycan-conjugated ADCs

Glycan-conjugated ADCs were prepared as described previously (*12*). Briefly, anti-PSMA antibody D2B (15 mg/mL) was incubated with 1% (w/w) of endoglycosidase in 20 mM Tris pH 7.5 for 16 h at 37 °C. Complete trimming was confirmed by mass spectral analysis on Fc/2 domain. After deconvolution of peaks, two major products were observed (24633 Da and 24761 Da) for the trimmed anti-PSMA antibody D2B, resulting from core GlcNAc(Fuc) and GlcNAc(Fuc) without lysine (-Lys) anti-PSMA D2B. The starting material showed three major products (25733 Da, 25859 Da and 26022 Da) corresponding to G_0F (-Lys), G_0F and G_1F, respectively.

Subsequently, trimmed anti-PSMA D2B (10 mg/mL) was incubated with 5 mM F_2-GalNAz (75 equivalent), 5% (w/w) glycosyltransferase (developed in house), 10 mM $MnCl_2$ in 20 mM Tris pH 7.5 for 16 h at 30 °C. Mass spectral analysis of anti-PSMA D2B antibody (F_2-GalNAz)$_2$ after FabULOUS and DTT treatment showed two major peaks corresponding to incorporated F_2-GalNAz with DTT as an adduct, 25000 Da (-Lys) and 25129 Da. The DTT-adduct is only a result of sample preparation for mass spectral analysis. The anti-PSMA D2B (F_2-GalNAz)$_2$ reaction mixture was loaded on a protein A column (endotoxin free) and the antibody was eluted with 0.1 M Glycine pH 2.7 followed by dialysis to PBS. The general protocol for conjugation of BCN (bicyclo[6.1.0]non-4yne), modified with either one or two toxic payloads (MMAE or duocarmycin) via a cleavable linker (Val-Cit-PABC), to anti-PSMA D2B (F_2-GalNAz)$_2$ was performed as follows. 4 mg of anti-PSMA D2B (F_2-GalNAz)$_2$ (12 mg/mL) was conjugated with 5-10 equivalent BCN-toxin in PBS and in presence of 25% DMF. The ADCs were purified by size exclusion chromatography (SEC) in PBS.

Mouse model

Animal experiments were conducted in accordance with the principles laid out by the revised Dutch Act on Animal Experimentation (2014) and approved by the institutional Animal Welfare Committee of the

Radboud University Nijmegen. Male BALB/c nude mice (Janvier), 7–8 wk old, were housed in individually ventilated filter-topped cages (5 mice per cage) under nonsterile standard conditions with free access to standard animal chow and water. After one week of adaptation to laboratory conditions, 3×10^6 PSMA-transfected LS174T cells (*17*) were suspended in 200 µL of complete RPMI 1640 medium and injected subcutaneously (right flank). LS174T-PSMA cells were grown in RPMI 1640 medium supplemented with 10% fetal calf serum (Life Technologies) and 2 mM glutamine.

Radiolabeling

The antibody-drug conjugates were conjugated with diethylenetriaminepentaacetic acid (DTPA) as described previously (*15*). Both DTPA-D2B-duocarmycin ADCs (108.2 µg) were radiolabeled with 120 MBq of ^{111}In (Mallinckrodt Pharmaceuticals, Cham, Switzerland), while DTPA-D2B and both DTPA-D2B-MMAE ADCs (96.1 µg) were radiolabeled with 106.7 MBq of ^{111}In in 0.1 M 2-(N-morpholino)ethanesulfonic acid buffer, pH 5.4 (3 times the volume of $^{111}InCl_3$), and incubated for 20 min at room temperature under metal-free conditions. Subsequently, 50 mM ethylenediaminetetraacetic acid was added to the final concentration of 5 mM to chelate unincorporated ^{111}In. The labeling efficiency was determined by instant thin-layer chromatography using 0.15 M citrate buffer, pH 6.0, as the mobile phase. The labeling efficiency was 85%. The ^{111}In-labeled agents were purified by gel filtration on a PD-10 column, and the radiochemical purity of the agents exceeded 95%, which was determined by instant thin-layer chromatography.

In vitro characterization

The immunoreactive fraction of ^{111}In-DTPA-D2B, ^{111}In-DTPA-D2B-DAR2-duocarmycin, ^{111}In-DTPA-D2B-DAR4-duocarmycin, ^{111}In-DTPA-D2B-DAR2-MMAE, and ^{111}In-DTPA-D2B-DAR4-MMAE were determined essentially as described by Lindmo et al. (*18*). A serial dilution of LS174T-PSMA cells ($3.3 \times 10^6 – 5.2 \times 10^7$

cells/mL) in RPMI-1640 containing 0.5% BSA was incubated with ^{111}In-D2B, ^{111}In-DTPA-D2B-DAR2-duocarmycin, ^{111}In-DTPA-D2B-DAR4-duocarmycin, ^{111}In-DTPA-D2B-DAR2-MMAE, or ^{111}In-DTPA-D2B-DAR4-MMAE. Nonspecific binding was determined by adding an excess of unlabeled D2B (5 µg) to a duplicate of the lowest cell concentration. After an incubation for 1 hour at 37 °C, cells were centrifuged and the activity in the cell pellet was measured in a γ counter (Wizard 3" 1480; LKB-Wallac, PerkinElmer). The inverse of the specific cell bound activity was plotted against the inverse of the cell concentration, and the immunoreactive fraction was calculated from the y-axis intercept using GraphPad Prism (version 5.03 for Windows).

LS174T-PSMA cells were cultured in six-well plates and were incubated with 1.9 kBq of ^{111}In-D2B, ^{111}In-DTPA-D2B-DAR2-duocarmycin, ^{111}In-DTPA-D2B-DAR4-duocarmycin, ^{111}In-DTPA-D2B-DAR2-MMAE, or ^{111}In-DTPA-D2B-DAR4-MMAE for 4, 24, and 48h in 2ml binding buffer at 37 °C in a humidified atmosphere with 5% CO_2. Nonspecific binding and internalization was determined by coincubation with unlabeled D2B. After incubation, acid wash buffer (0.1 M HAc, 0.15 M NaCl, pH2.6) was added for 10 min to remove the membrane-bound fraction of the cell-associated ^{111}In-labeled compounds. Subsequently, cells were harvested from the six-well plates and the amount of membrane-bound and internalized activity was measured in a gamma counter.

MicroSPECT/CT imaging and ex vivo biodistribution

20 male BALB/c nude mice (5 mice per agent) with PSMA-expressing LS174T-PSMA tumors (right flank) were injected into the tail vein with 25 µg of ^{111}In-DTPA-D2B-DAR2-duocarmycin (21.9 ± 0.6 MBq), ^{111}In-DTPA-D2B-DAR4-duocarmycin (21.8 ± 0.9 MBq), ^{111}In-DTPA-D2B-DAR2-MMAE (17.0 ± 0.7 MBq), or ^{111}In-DTPA-D2B-DAR4-MMAE (15.0 ± 0.4 MBq). Five additional mice were injected intravenously with 25 µg of ^{111}In-DTPA-D2B (17.3 ± 0.6 MBq) serving as a reference group to determine the biodistribution of unmodified D2B. At 3 days after injection, mice were euthanized with CO_2/O_2 asphyxiation. Of each

group, 2 mice underwent microSPECT/CT imaging (acquisition time 30 min), using small-animal microSPECT/CT scanner (U-SPECT II; MILabs) using the 1.0 mm diameter pinhole mouse high sensitivity collimator tube, followed by a CT scan (spatial resolution 160 µm, 65 kV, 615 µA) for anatomical reference. Scans were reconstructed with MILabs reconstruction software, using an ordered-subset expectation maximization algorithm, energy window 154 - 188 keV, 3 iterations, 16 subsets, and voxel size of 0.2 mm, and Gaussian filter 0.4 mm. SPECT/CT scans were analyzed and maximum intensity projections (MIPs) were created using the Inveon Research Workplace software (IRW, version 4.1). For each mouse, tissues of interest (LS174T-PSMA tumors, muscle, lung, spleen, kidney, liver, small intestine, salivary glands, and adrenals) were dissected and weighed, followed by measurements of the radioactivity in a γ counter. Blood samples were obtained by heart puncture. To calculate radioactivity uptake in tissue as a fraction of the injected dose, an aliquot of the injected dose was counted simultaneously.

Therapeutic efficacy of ADCs

Sixty mice were inoculated subcutaneously with PSMA-transfected LS174T cells. When the tumors reached a size of approximately 100 mm^3, mice were randomly assigned into six groups and received a single dose of 5 mg/kg ADC, unconjugated D2B, or PBS. Tumor size and body weight were measured two times per week by a technician who was blinded for the treatment groups. Mice were taken out of the experiment if one of the following end points was reached: tumor volume of ≥ 500 mm^3, decrease in body weight ≥20% compared to baseline or ≥15% in two days, ulceration or invasive tumor growth.

Statistical analysis

Differences in tumor uptake, blood concentration, tumor-to-blood ratios, and tumor doubling time between ^{111}In-DTPA-D2B, ^{111}In-DTPA-D2B-DAR2-duocarmycin and ^{111}In-DTPA-D2B-DAR4-duocarmycin or

^{111}In-DTPA-D2B-DAR2-MMAE and ^{111}In-DTPA-D2B-DAR4-MMAE were tested for significance via one-way analysis of variance and Bonferroni's multiple comparison post analysis using GraphPad Prism version 5.03 (San Diego, CA). Survival was described with the median survival, and survival curves were compared with the log-rank (Mantel-Cox) test using GraphPad Prism version 5.03. A p-value below 0.05 was considered significant.

RESULTS

D2B-ADCs specifically bind to PSMA-expressing cells

The immunoreactive fractions of ^{111}In-D2B, ^{111}In-DTPA-D2B-DAR2-duocarmycin, ^{111}In-DTPA-D2B-DAR4-duocarmycin, ^{111}In-DTPA-D2B-DAR2-MMAE, and ^{111}In-DTPA-D2B-DAR4-MMAE were 69.3, 86.5, 75.5, 68.4, and 78.0%, respectively, indicating that the immunoreactivity of the D2B antibody was preserved during the conjugation procedures. Maximum binding to PSMA-expressing LS174T-PSMA cells reached 74 – 80% for the reference compound and all D2B-based drug conjugates (**figure 1**).

D2B-ADCs gradually internalize into PSMA-expressing cells

All radiolabeled D2B-ADCs including native D2B gradually and specifically internalized into PSMA-expressing LS174T-PSMA cells, although absolute binding and internalization of ^{111}In-DTPA-D2B-DAR2-MMAE and ^{111}In-DTPA-D2B-DAR4-MMAE was higher compared to native ^{111}In-DTPA-D2B, ^{111}In-DTPA-D2B-DAR2-duocarmycin, and ^{111}In-DTPA-D2B-DAR4-duocarmycin. During the first 24h of incubation, all compounds were mainly membrane bound. The internalized fraction gradually increased until 48h of incubation, reaching 25.4 ± 1.3 %, 27.9 ± 0.7 %, 25.4 ± 1.3 %, 31.8 ± 0.9 %, and 31.4 ± 1.5 % of the total cell-associated activity of ^{111}In-DTPA-D2B, ^{111}In-DTPA-D2B-DAR2-duocarmycin, ^{111}In-DTPA-D2B-DAR4-duocarmycin, ^{111}In-DTPA-D2B-DAR2-MMAE, and ^{111}In-DTPA-D2B-DAR4-MMAE, respectively.

D2B-ADC efficiently accumulate in PSMA-expressing tumors

10 BALB/c nude mice with s.c. LS174T-PSMA tumors were imaged with the microSPECT/CT scanner at 3 days after injection of ^{111}In-DTPA-D2B-DAR2-duocarmycin, ^{111}In-DTPA-D2B-DAR4-duocarmycin, ^{111}In-DTPA-D2B-DAR2-MMAE, ^{111}In-DTPA-D2B-DAR4-MMAE, or ^{111}In-DTPA-D2B. A typical set of microSPECT/CT acquisitions is shown in **figure 2**. LS174T-PSMA tumors were clearly visualized by microSPECT/CT imaging with homogenous uptake for all four ^{111}In-labeled ADCs. On microSPECT/CT images, liver uptake of the duocarmycin variants seemed to be higher compared to the MMAE variants.

Ex vivo biodistribution revealed that all ADCs showed high accumulation in PSMA-positive LS174T-PSMA tumors (**table 1**). Tumor uptake of ^{111}In-DTPA-D2B-DAR2-MMAE (119.7 ± 37.4 %ID/g) was significantly higher at 3 days post injection than that of the reference compound ^{111}In-DTPA-D2B, (75.1 ± 8.1%ID/g, $p<0.05$). In addition, tumor uptake of ^{111}In-DTPA-D2B-DAR2-MMAE (119.7 ± 37.4 %ID/g) was significantly higher than that of ^{111}In-DTPA-D2B-DAR4-MMAE (62.1 ± 21.1 %ID/g) and ^{111}In-DTPA-D2B-DAR4-duocarmycin (70.7 ± 15.1 %ID/g) at 3 days after injection ($p<0.01$ and $p<0.05$, respectively). No significant difference in tumor uptake was observed between the reference compound ^{111}In-DTPA-D2B (75.1 ± 8.1 %ID/g), ^{111}In-DTPA-D2B-DAR2-duocarmycin (87.7 ± 15.4 %ID/g), and ^{111}In-DTPA-D2B-DAR4-duocarmycin (70.7 ± 15.1 %ID/g) (**figure 3**).

The uptake of ^{111}In-DTPA-D2B-DAR2-duocarmycin and ^{111}In-DTPA-D2B-DAR4-duocarmycin remained low in most normal tissues; hepatic uptake reached 5.0 ± 1.2 %ID/g and 7.4 ± 2.4 %ID/g at 3 days after injection, respectively, while kidney uptake reached 4.2 ± 0.5 %ID/g and 4.1 ± 0.4 %ID/g. For ^{111}In-DTPA-D2B-DAR2-MMAE and ^{111}In-DTPA-D2B-DAR4-MMAE, hepatic uptake was 4.9 ± 1.3 and 4.8 ± 1.3 %ID/g (n = 5), while kidney uptake was 6.5 ± 1.5 %ID/g and 7.0 ± 1.7 %ID/g, respectively. Hepatic uptake between the reference compound ^{111}In-DTPA-D2B and ^{111}In-DTPA-D2B-DAR2-duocarmycin, ^{111}In-

DTPA-D2B-DAR4-duocarmycin, ^{111}In-DTPA-D2B-DAR2-MMAE or ^{111}In-DTPA-D2B-DAR4-MMAE was not significantly different.

^{111}In-DTPA-D2B-DAR2-MMAE showed significantly higher blood levels at 3 days p.i. compared to the reference compound ^{111}In-DTPA-D2B (18.6 ± 4.7 %ID/g and 12.2 ± 1.1 %ID/g, respectively, $p<0.01$) as well as compared to ^{111}In-DTPA-D2B-DAR4-MMAE (8.8 ± 2.2 %ID/g, $p<0.001$). In addition, ^{111}In-DTPA-D2B-DAR2-MMAE showed significantly higher blood levels compared to ^{111}In-DTPA-D2B-DAR2-duocarmycin (11.4 ± 0.9 %ID/g, $p<0.01$), and ^{111}In-DTPA-D2B-DAR4-duocarmycin (10.3 ± 1.5 %ID/g, $p<0.001$). No significant difference in tracer concentration in the blood was observed between the reference compound ^{111}In-DTPA-D2B and ^{111}In-DTPA-D2B-DAR4-MMAE, ^{111}In-DTPA-D2B-DAR2-duocarmycin, or ^{111}In-DTPA-D2B-DAR4-duocarmycin.

However, tumor-to-blood ratios of ^{111}In-DTPA-D2B-DAR2-duocarmycin (6.5 ± 1.3), ^{111}In-DTPA-D2B-DAR4-duocarmycin (7.3 ± 2.3), ^{111}In-DTPA-D2B-DAR2-MMAE (7.7 ± 1.2), and ^{111}In-DTPA-D2B-DAR4-MMAE (7.0 ± 1.9) at 3 days postinjection did not differ significantly from each other and from that of the reference compound ^{111}In-DTPA-D2B (6.2 ± 0.7).

Tumor growth is inhibited by D2B-ADCs

Body weight and tumor size between the treatment groups at the beginning of treatment was not significantly different. Tumor growth after treatment with PBS, unmodified D2B, D2B-DAR2-duocarmycin, D2B-DAR4-duocarmycin, D2B-DAR2-MMAE, and D2B-DAR4-MMAE in individual mice is depicted in **figure 4**. Longest tumor doubling time was observed after treatment with D2B-DAR4-MMAE (9.2 ± 2.1 days), which was significantly longer than that in the PBS control mice (3.5 ± 0.5 days, $p<0.001$), unmodified D2B (4.2 ± 2.0 days, $p<0.001$), D2B-DAR2-MMAE (5.2 ± 1.8 days, $p<0.001$), D2B-DAR2-duocarmycin (3.9 ± 2.7 days, $p<0.001$), and D2B-DAR4-duocarmycin (3.6 ± 0.8 days, $p<0.001$)

(**figure 5b**). Tumor doubling time did not significantly differ in mice that received PBS only, unmodified D2B, D2B-DAR2-MMAE, D2B-DAR2-duocarmycin, and D2B-DAR4-duocarmycin.

Median survival of the control mice that received PBS was 13 days. Median survival of mice treated with D2B in its unmodified form was not significantly different: 17 days, indicating that unmodified D2B alone has no therapeutic effect. Treatment with D2B-DAR2-duocarmycin (median survival 15 days) and D2B-DAR4-duocarmycin (median survival 13 days) did not prolong median survival significantly compared to treatment with PBS or D2B alone (Mantel Cox test, p=0.8884) (**figure 5a**). Treatment with D2B-DAR4-MMAE and D2B-DAR2-MMAE significantly improved median survival from 13 to 29 ($p<0.001$) and 20 days ($p<0.01$), respectively (**figure 5a**). No significant difference in median survival was observed between treatment with D2B-DAR4-MMAE and D2B-DAR2-MMAE. Treatment with D2B-DAR4-MMAE resulted in significantly prolonged median survival compared to treatment with D2B-DAR2-duocarmycin ($p<0.05$) and D2B-DAR4-duocarmycin ($p<0.001$). Moreover, treatment with D2B-DAR2-MMAE resulted in significantly prolonged median survival compared to treatment with D2B-DAR2-duocarmycin ($p<0.01$) and D2B-DAR4-duocarmycin ($p<0.001$).

DISCUSSION

This report describes the in vitro and in vivo characterization of four novel site-specifically conjugated anti-PSMA ADCs consisting of the anti-PSMA mAb D2B conjugated to either 2 or 4 molecules of duocarmycin or MMAE.

So far, the majority of the tested anti-PSMA ADCs is based on random conjugation of the drug to the antibody, resulting in mixtures of ADCs with different molar DARs, linked at different sites to the antibody and with different pharmacokinetics, immunoreactivity, charge, size, and stability (*13*). In addition, in randomly conjugated ADCs, DAR0 species can occur, which do not contribute to drug-

mediated anti-tumor activity and compete for antigen-binding sites with higher DAR species (*19*). So far, several strategies have been developed to improve the therapeutic efficacy of ADCs, among which the site-specific conjugation of antibodies to cytotoxic drugs (*13,20*). This strategy is based on providing an anchor point in the antibody molecule for attachment of the drug, which allows specific conjugation to a certain point in the molecule structure preventing random binding. It was shown previously that site-specific conjugation minimizes heterogeneity of ADCs, rendering the properties of ADCs more predictable, allowing consistent conjugate production (*20*). In addition, it was shown that engineered site-specific ADC conjugates were better tolerated in both rat and cynomolgus monkey toxicity models compared with traditional ADC conjugates (*13,20,21*), presumably because these ADCs do not disintegrate in vivo as much as non-site specifically conjugated ADCs.

Recently, van Geel and colleagues developed a method to site-specifically conjugate ADCs using the antibody's glycan at asparagine-297 as an anchor (GlycoConnect™ method) (*12*). Major advantages of this method are that it is applicable to any type of recombinant IgG isotype, irrespective of mammalian expression system and linker–payload combination (*12*). ADCs produced by this method were found to be homogeneous and hydrolytically stable, while displaying negligible aggregation (*12*). In addition, immunoreactivity is preserved entirely, as the drug is conjugated to the antibody at a site not affecting antigen binding/affinity. Glycan-remodeled trastuzumab showed significantly improved anti-tumor activity compared to the clinically available ADC Kadcyla® demonstrating the superiority of GlycoConnect™ ADC versus a randomly conjugated ADC based on the same components (*12*).

In addition to site-specific conjugation, it has been shown that the anti-tumor effect of ADCs can be modified by varying the drug loading per antibody (*22*). Hamblett and colleagues demonstrate that a single dose of an ADC with a DAR of 2 can be less effective than treatment with an ADC with a DAR of 4. In contrast, it was shown that ADCs containing higher DAR species (DAR6 and DAR8) are generally less stable and clear more rapidly compared to lower DAR species, depending on the conjugation method

(*22*). Therefore, in the present study, we concentrated on the evaluation of anti-tumor activity of DAR2 and DAR4 species.

Previously, it was shown that the number of drug molecules that can be conjugated to an antibody molecule is also limited as it can reduce the antigen binding capacity by blocking binding sites (*23*). In the present study, in vitro, the immunoreactivity of the anti-PSMA mAb D2B was preserved upon site-specific conjugation with MMAE or duocarmycin and all four ADC conjugates show comparable binding to PSMA-expressing cells as D2B IgG, thereby demonstrating that site-specific conjugation does not interfere with antigen binding. Binding capacity of the different anti-PSMA ADCs to PSMA-expressing tumor cells was not significantly different from each other and from the unmodified D2B antibody.

In vivo, microSPECT/CT images allowed high-contrast visualization of PSMA-expressing tumors for all four ADC variants. Tumor visualization was comparable to that using the reference compound ^{111}In-D2B, confirming in vivo tumor targeting remains intact upon conjugation to the ADCs. ^{111}In-labeled anti-PSMA ADCs showed a biodistribution profile comparable to ^{111}In-D2B with high tumor uptake and relatively low uptake in healthy organs. Highest tumor uptake however was reached with the D2B-DAR2-MMAE variant, which was significantly increased in comparison to unmodified D2B as well as the D2B-DAR4-variant, which might be explained by altered pharmacokinetics of the different DAR variants in vivo. The D2B-DAR2-MMAE variant showed significantly prolonged blood circulation compared to all other variants, which may have resulted in increased tumor uptake. Differences in blood circulation have been described previously for ADCs with different DARs. ADC with higher DAR, especially MMAE ADCs, clear more rapidly from the circulation compared to ADC species with lower DAR (*22,24*). Explanation for this observation is most likely the enhanced liver clearance of the higher conjugated species, due to the hydrophobic nature of the payload, leading to alterations in pharmacokinetics.

Subsequently, anti-tumor activity of MMAE- and duocarmycin-based anti-PSMA ADCs in terms of median survival and tumor doubling time was compared to that of mice that received PBS or D2B

without addition of a cytotoxic drug. Both MMAE-based anti-PSMA ADCs significantly prolonged median survival. As the DAR4 variant carries more cytotoxic drugs than the DAR2 variant, the DAR4 variant was expected to have higher anti-tumor activity compared to the DAR2 variant (*22*). Indeed, tumor doubling time of D2B-DAR4-MMAE was significantly higher than that of D2B-DAR2-MMAE. However, no significant difference in prolongation of median survival was observed between D2B-DAR2-MMAE and D2B-DAR4-MMAE. An explanation for this could be the prolonged circulation time and increased tumor uptake of the D2B-DAR2-variant, leading effectively to relatively more intracellular free toxin and thereby compensating for the absolute lower number of cytotoxic drugs carried.

No significant difference between the DAR2 and DAR4 variant of the duocarmycin-based anti-PSMA ADC was observed; in contrast to the D2B-DAR2-MMAE and D2B-DAR4-MMAE variants, neither leading to prolonged tumor doubling time nor median survival. While MMAE inhibits microtubule assembly, ultimately precluding mitosis and causing apoptosis in dividing tumor cells, duocarmycin acts in both dividing and nondividing cells as it alkylates DNA resulting in DNA damage, mitochondrial stress, impaired DNA transcription, apoptosis, and ultimately cell death. Based on these mechanisms, both duocarmycin and MMAE are expected to have high anti-tumor activity. Lack of anti-tumor activity of the duocarmycin-based ADCs might be explained by relatively slower onset of DNA-damaging agents versus micotubuli inhibitors in rapidly dividing cells as those used in the present study. Moreover, lower anti-tumor activity of duocarmycin might be a consequence of the requirement of this drug to arrive to the nucleous for developing its activity while MMAE acts in the cytoplasm. In addition, structural changes due to conjugation of the drug to the antibody might cause reduced internalization of the ADC or diminished lysosomal degradation (*25*). In the present study, mice received a single dose of 5 mg/kg of the ADC. While no maximum tolerable dose was determined here, Owonikoko et al. report that side effects such as neuropathy occur at doses of 15 mg/kg of BMS936561, an ADC consisting of an anti-CD70 antibody covalently linked to duocarmycin (*26*). In this study, the authors report 8 mg/kg to be the best

tolerated dose (*26*). This suggests that upscaling of the dose of the here evaluated duocarmycin-based ADCs could be well tolerated. Therapeutic effect of these duocarmycin-based ADCs should be evaluated at higher doses. Aggressive tumor growth of PSMA-expressing LS174T-PSMA tumor cells may have masked less pronounced treatment effects. Therefore, in future therapy studies, a tumor model that shows a less aggressive growth pattern should be evaluated as well. Finally, it is important to point out that although we treated the tumor bearing mice with only one dose of our DAB2-DAR4-MMAE ADC we obtained a doubling of the survival time in our fast growing tumor model. It is well-known that the therapeutic strategies to destroy tumor cells are based on repeated administration of the drugs in order to improve the anti-tumor efficacy, so in future, efficacy of this new treatment should be evaluated with repeated ADC administration cycles in order to increase the anti-tumor response.

CONCLUSION

In this study, site-specifically conjugated MMAE- and duocarmycin-based anti-PSMA ADCs with different DARs have been characterized. While the duocarmycin-based anti-PSMA ADCs did not show anti-tumor activity at the dose used in this study, the site-specifically conjugated anti-PSMA ADCs D2B-DAR2-MMAE and D2B-DAR4-MMAE effectively inhibited tumor growth of PSMA-expressing tumors and prolonged survival of the mice. Highest anti-tumor activity was achieved with the MMAE-based anti-PSMA ADC containing four molecules of MMAE per antibody molecule.

DISCLOSURE

The authors declare that they have no conflict of interest.

ACKNOWLEDGEMENTS

We thank Bianca Lemmers-van de Weem, Iris Lamers-Elemans, Kitty Lemmens-Hermans, and Karin de Haas-Cremers for technical assistance with the animal experiments. Furthermore, we thank Synaffix for making the conjugation technology available.

REFERENCES

1. Mottet N, Bellmunt J, Bolla M, et al. EAU-ESTRO-SIOG Guidelines on Prostate Cancer. Part 1: Screening, Diagnosis, and Local Treatment with Curative Intent. *Eur Urol.* 2016.

2. Denmeade SR, Isaacs JT. A history of prostate cancer treatment. *Nat Rev Cancer.* 2002;2:389-396.

3. Gulley J, Dahut WL. Chemotherapy for prostate cancer: finally an advance! *Am J Ther.* 2004;11:288-294.

4. Wang X, Ma D, Olson WC, Heston WD. In vitro and in vivo responses of advanced prostate tumors to PSMA ADC, an auristatin-conjugated antibody to prostate-specific membrane antigen. *Mol Cancer Ther.* 2011;10:1728-1739.

5. Ma D, Hopf CE, Malewicz AD, et al. Potent antitumor activity of an auristatin-conjugated, fully human monoclonal antibody to prostate-specific membrane antigen. *Clin Cancer Res.* 2006;12:2591-2596.

6. Vaishampayan U, Glode M, Du W, et al. Phase II study of dolastatin-10 in patients with hormone-refractory metastatic prostate adenocarcinoma. *Clin Cancer Res.* 2000;6:4205-4208.

7. Pandit-Taskar N, O'Donoghue JA, Divgi CR, et al. Indium 111-labeled J591 anti-PSMA antibody for vascular targeted imaging in progressive solid tumors. *EJNMMI Res.* 2015;5:28.

8. Lutje S, Sauerwein W, Lauenstein T, Bockisch A, Poeppel TD. In Vivo Visualization of Prostate-Specific Membrane Antigen in Adenoid Cystic Carcinoma of the Salivary Gland. *Clin Nucl Med.* 2016;41:476-477.

9. Lutje S, Gomez B, Cohnen J, et al. Imaging of Prostate-Specific Membrane Antigen Expression in Metastatic Differentiated Thyroid Cancer Using 68Ga-HBED-CC-PSMA PET/CT. *Clin Nucl Med.* 2017;42:20-25.

10. Kuroda K, Liu H, Kim S, Guo M, Navarro V, Bander NH. Saporin toxin-conjugated monoclonal antibody targeting prostate-specific membrane antigen has potent anticancer activity. *Prostate.* 2010;70:1286-1294.

11. Milowsky MI, Galsky MD, Morris MJ, et al. Phase 1/2 multiple ascending dose trial of the prostate-specific membrane antigen-targeted antibody drug conjugate MLN2704 in metastatic castration-resistant prostate cancer. *Urol Oncol.* 2016;34:530 e515-530 e521.

12. van Geel R, Wijdeven MA, Heesbeen R, et al. Chemoenzymatic Conjugation of Toxic Payloads to the Globally Conserved N-Glycan of Native mAbs Provides Homogeneous and Highly Efficacious Antibody-Drug Conjugates. *Bioconjug Chem.* 2015;26:2233-2242.

13. Junutula JR, Raab H, Clark S, et al. Site-specific conjugation of a cytotoxic drug to an antibody improves the therapeutic index. *Nat Biotechnol.* 2008;26:925-932.

14. Shen BQ, Xu K, Liu L, et al. Conjugation site modulates the in vivo stability and therapeutic activity of antibody-drug conjugates. *Nat Biotechnol.* 2012;30:184-189.

15. Lutje S, van Rij CM, Franssen GM, et al. Targeting human prostate cancer with 111In-labeled D2B IgG, F(ab')2 and Fab fragments in nude mice with PSMA-expressing xenografts. *Contrast Media Mol Imaging.* 2015;10:28-36.

16. Elgersma RC, Coumans RG, Huijbregts T, et al. Design, Synthesis, and Evaluation of Linker-Duocarmycin Payloads: Toward Selection of HER2-Targeting Antibody-Drug Conjugate SYD985. *Mol Pharm.* 2015;12:1813-1835.

17. Lutje S, Rijpkema M, Franssen GM, et al. Dual-Modality Image-Guided Surgery of Prostate Cancer with a Radiolabeled Fluorescent Anti-PSMA Monoclonal Antibody. *J Nucl Med.* 2014;55:995-1001.

18. Lindmo T, Boven E, Cuttitta F, Fedorko J, Bunn PA, Jr. Determination of the immunoreactive fraction of radiolabeled monoclonal antibodies by linear extrapolation to binding at infinite antigen excess. *J Immunol Methods.* 1984;72:77-89.

19. Dokter W, Ubink R, van der Lee M, et al. Preclinical profile of the HER2-targeting ADC SYD983/SYD985: introduction of a new duocarmycin-based linker-drug platform. *Mol Cancer Ther.* 2014;13:2618-2629.

20. Panowski S, Bhakta S, Raab H, Polakis P, Junutula JR. Site-specific antibody drug conjugates for cancer therapy. *MAbs.* 2014;6:34-45.

21. Junutula JR, Flagella KM, Graham RA, et al. Engineered thio-trastuzumab-DM1 conjugate with an improved therapeutic index to target human epidermal growth factor receptor 2-positive breast cancer. *Clin Cancer Res.* 2010;16:4769-4778.

22. Hamblett KJ, Senter PD, Chace DF, et al. Effects of drug loading on the antitumor activity of a monoclonal antibody drug conjugate. *Clin Cancer Res.* 2004;10:7063-7070.

23. McCombs JR, Owen SC. Antibody drug conjugates: design and selection of linker, payload and conjugation chemistry. *AAPS J.* 2015;17:339-351.

24. Kamath AV, Iyer S. Preclinical Pharmacokinetic Considerations for the Development of Antibody Drug Conjugates. *Pharm Res.* 2015;32:3470-3479.

25. Barok M, Joensuu H, Isola J. Trastuzumab emtansine: mechanisms of action and drug resistance. *Breast Cancer Res.* 2014;16:209.

26. Owonikoko TK, Hussain A, Stadler WM, et al. First-in-human multicenter phase I study of BMS-936561 (MDX-1203), an antibody-drug conjugate targeting CD70. *Cancer Chemother Pharmacol.* 2016;77:155-162.

FIGURES

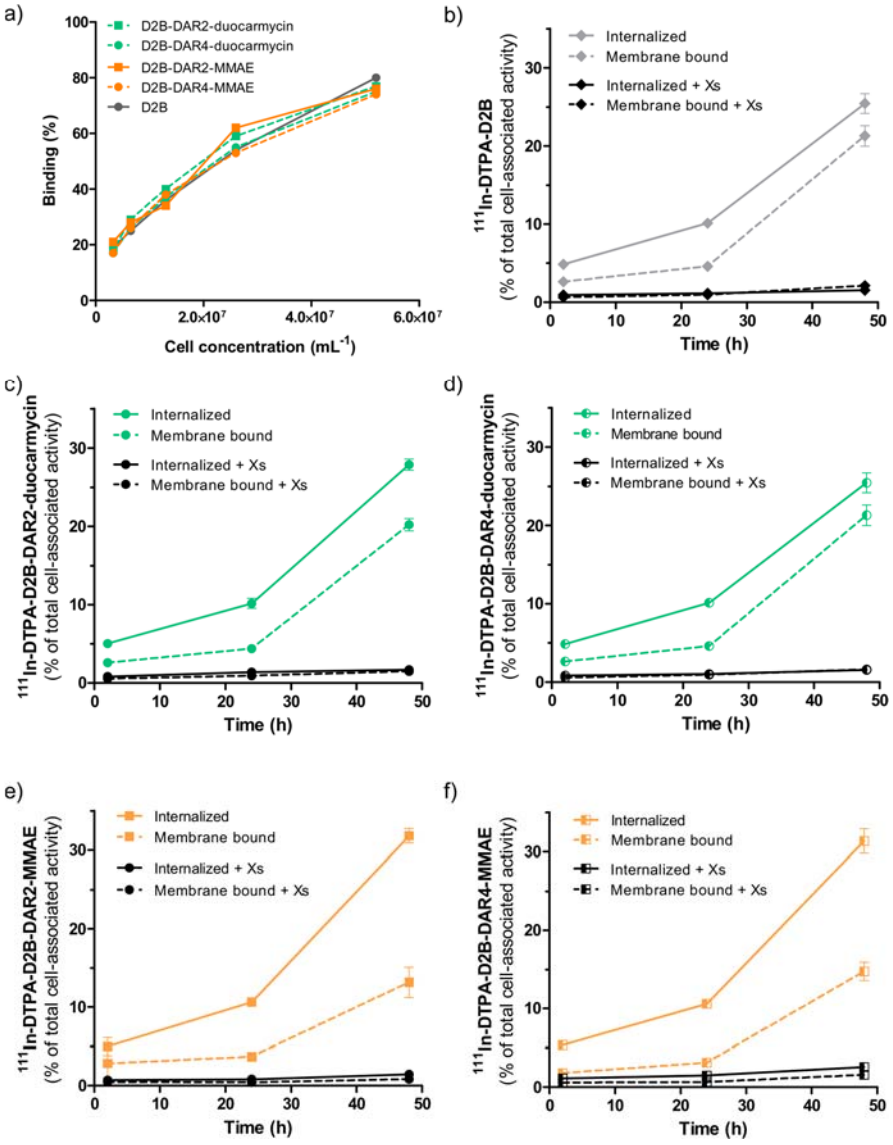

Figure 1: a) Binding of ^{111}In-D2B, ^{111}In-DTPA-D2B-DAR2-duocarmycin, ^{111}In-DTPA-D2B-DAR4-duocarmycin, ^{111}In-DTPA-D2B-DAR2-MMAE, and ^{111}In-DTPA-D2B-DAR4-MMAE to PSMA-expressing LS174T-PSMA cells. No significant difference in immunoreactivity of all five agents was observed. Internalization kinetics of ^{111}In-D2B (b), ^{111}In-DTPA-D2B-DAR2-duocarmycin (c), ^{111}In-DTPA-D2B-DAR4-duocarmycin (d), ^{111}In-DTPA-D2B-DAR2-MMAE (e), and ^{111}In-DTPA-D2B-DAR4-MMAE (f) in LS174T-PSMA cells. Binding and internalization is presented as the percentage of the total cell associated activity after 48h of incubation (mean ± SD).

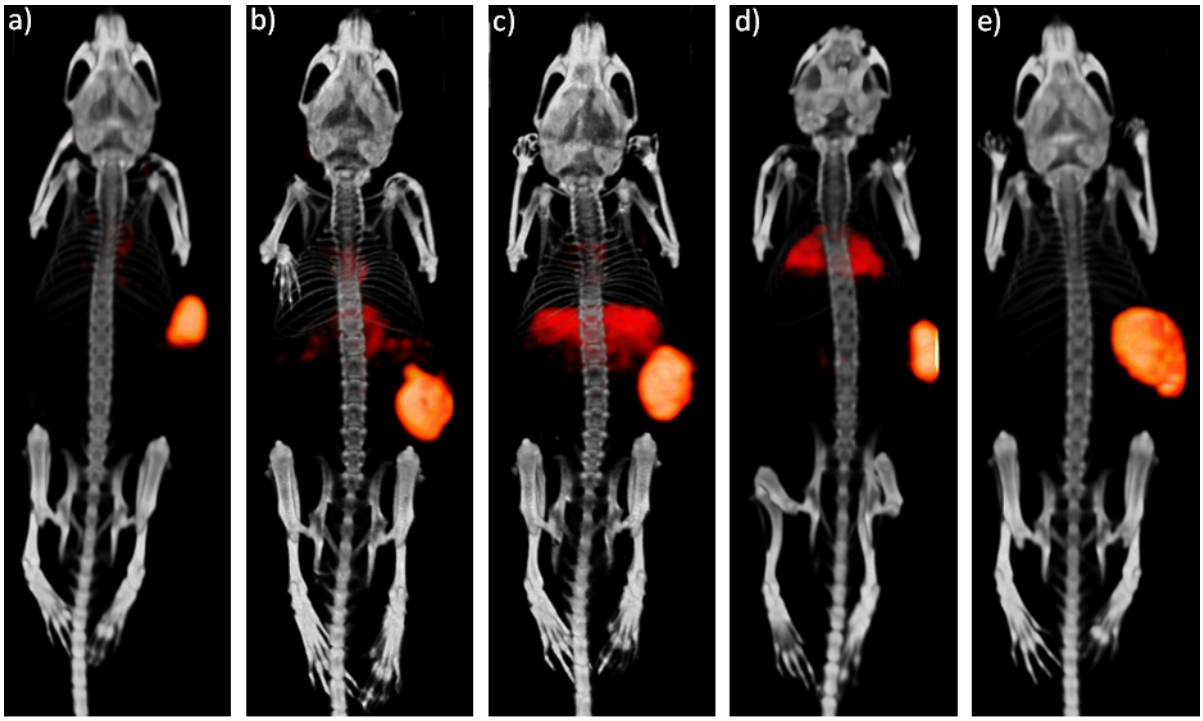

Figure 2: Representative microSPECT/CT images of mice with s.c. LS174T-PSMA xenografts on the right flank acquired 3 days after injection of a) ^{111}In-DTPA-D2B (17.8 MBq), b) ^{111}In-DTPA-D2B-DAR2-duocarmycin (22.1 MBq), c) ^{111}In-DTPA-D2B-DAR4-duocarmycin (20.8 MBq), d) ^{111}In-DTPA-D2B-DAR2-MMAE (17.2 MBq), and e) ^{111}In-DTPA-D2B-DAR4-MMAE (15.2 MBq).

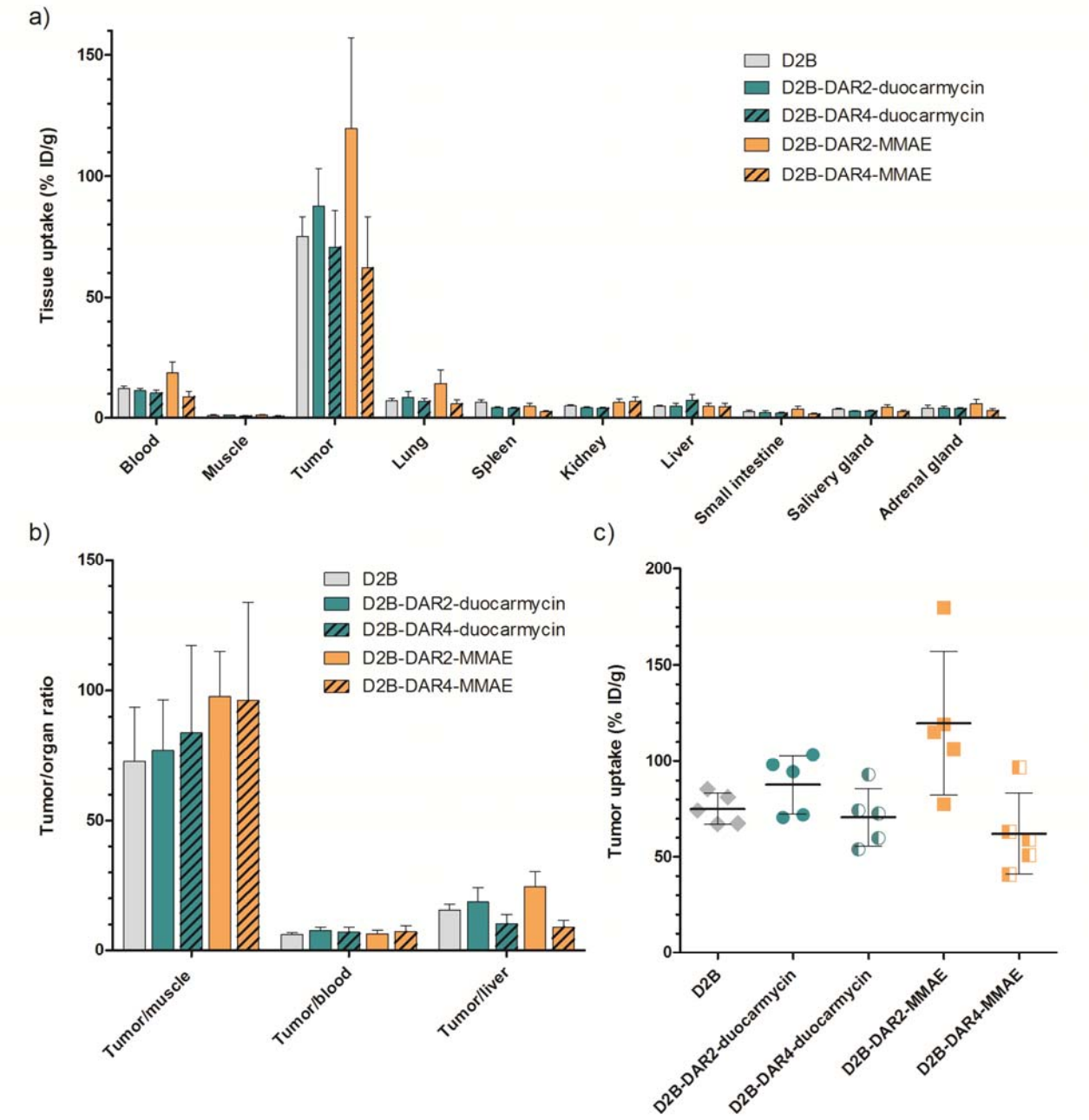

Figure 3: a) Biodistribution of ^{111}In-DTPA-D2B, ^{111}In-DTPA-D2B-DAR2-duocarmycin, ^{111}In-DTPA-D2B-DAR4-duocarmycin, ^{111}In-DTPA-D2B-DAR2-MMAE, and ^{111}In-DTPA-D2B-DAR4-MMAE in PSMA-expressing LS174T-PSMA tumors and healthy organs at 3 days after injection (n=5 mice per group). b) Tumor-to-organ ratios of all four agents and the control agent D2B, c) tumor uptake per mouse and targeting agent.

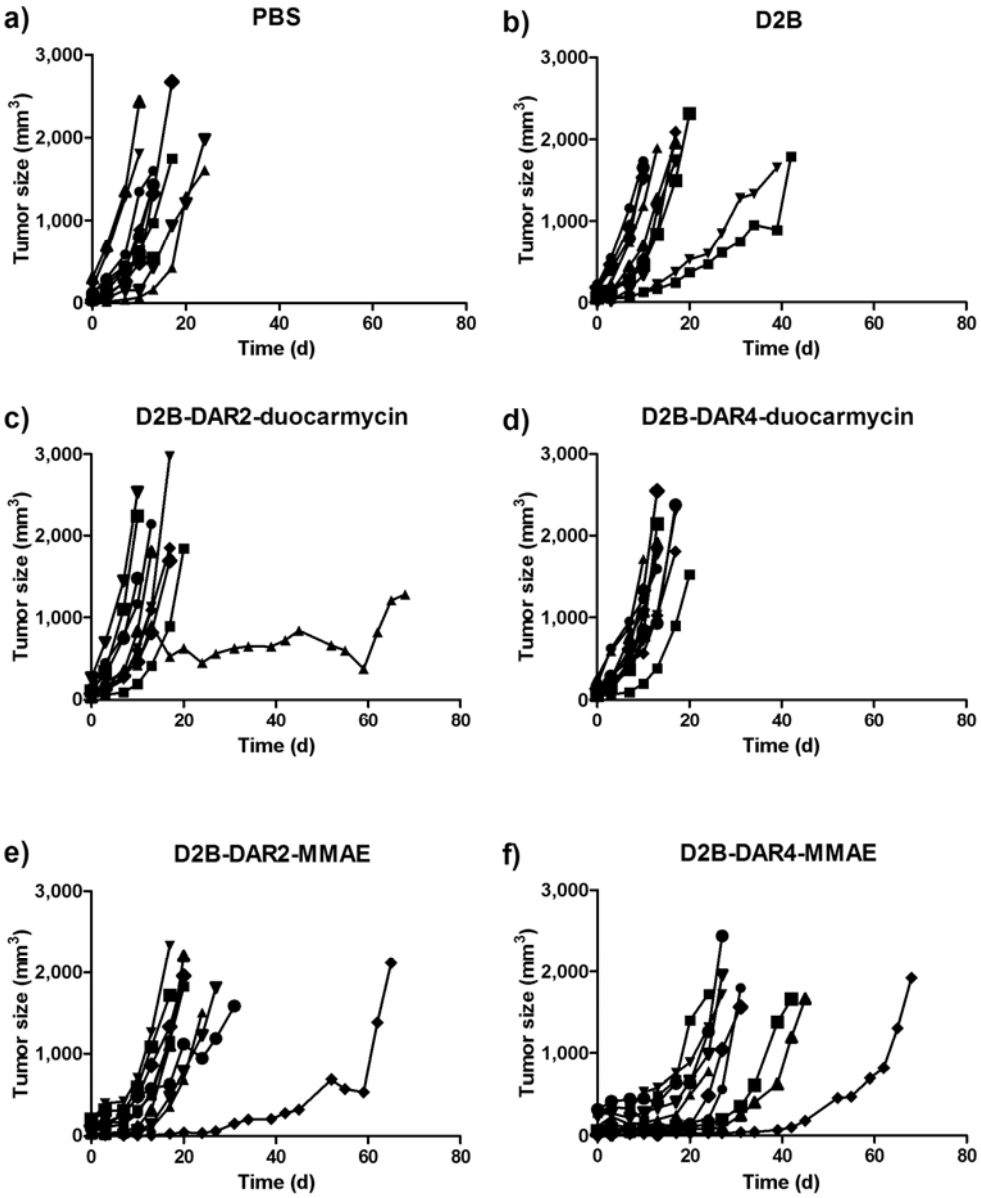

Figure 4: Tumor size of the individual mice in each group after treatment with PBS, D2B, D2B-DAR2-duocarmycin, D2B-DAR4-duocarmycin, D2B-DAR2-MMAE, or D2B-DAR4-MMAE (5 mg/kg).

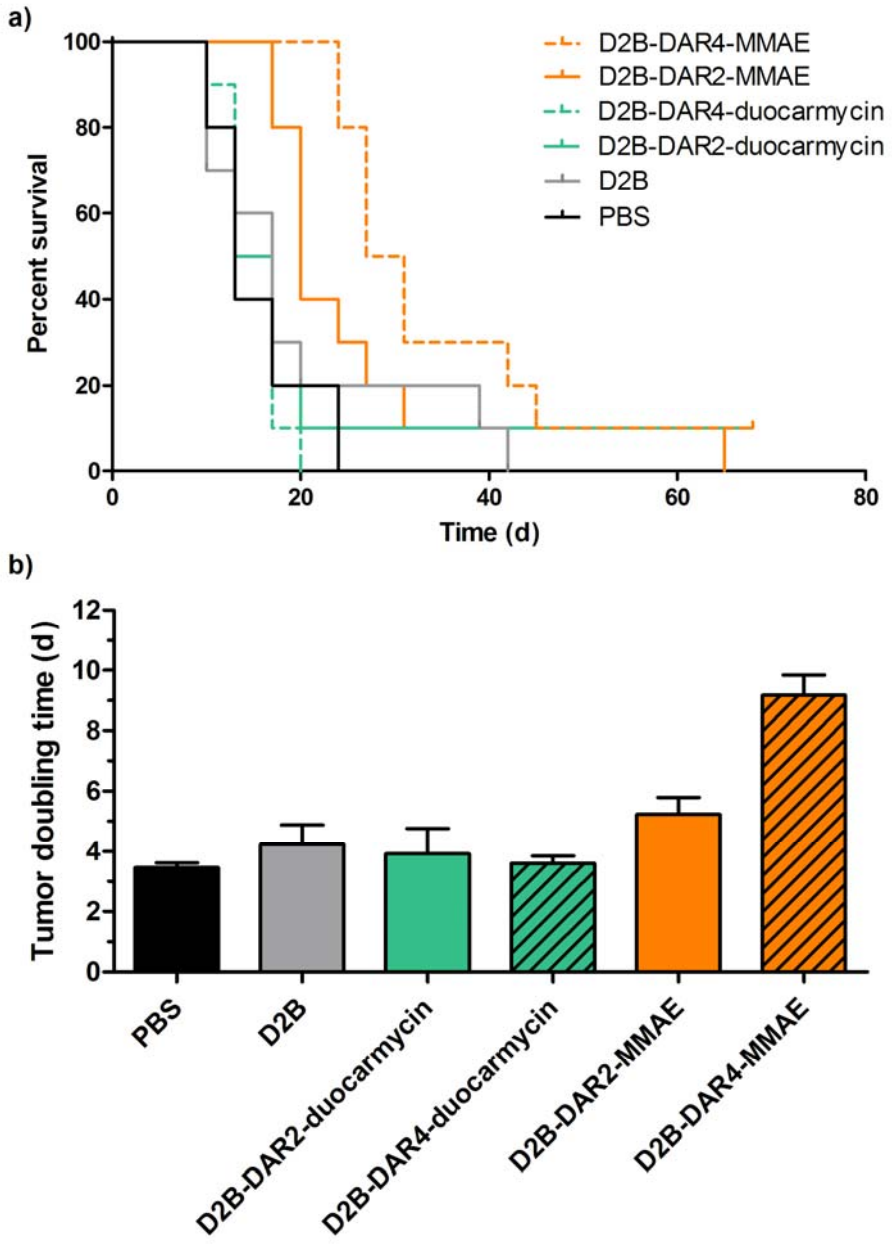

Figure 5: a) Kaplan-Meier survival plot of mice with s.c. LS174T-PSMA tumors treated with PBS, D2B, D2B-DAR2-duocarmycin, D2B-DAR4-duocarmycin, D2B-DAR2-MMAE, or D2B-DAR4-MMAE. b) Tumor-doubling time.

TABLES

Table 1: Biodistribution of ^{111}In-DTPA-D2B, ^{111}In-DTPA-D2B-DAR2-duocarmycin, ^{111}In-DTPA-D2B-DAR4-duocarmycin, ^{111}In-DTPA-D2B-DAR2-MMAE, and ^{111}In-DTPA-D2B-DAR4-MMAE at 3 days after injection (n=5 mice per group), data are represented in mean ± SD.

Organ	D2B	D2B-DAR2-duocarmycin	D2B-DAR4-duocarmycin	D2B-DAR2-MMAE	D2B-DAR4-MMAE
Blood	12.2 ± 1.1	11.4 ± 0.9	10.3 ± 1.5	18.6 ± 4.7	8.8 ± 2.2
Muscle	1.1 ± 0.3	1.2 ± 0.1	0.9 ± 0.2	1.2 ± 0.3	0.7 ± 0.3
Tumor	75.1 ± 8.1	87.7 ± 15.4	70.7 ± 15.1	119.7 ± 37.4	62.1 ± 21.1
Lung	7.1 ± 1.1	8.6 ± 2.3	7.0 ± 1.2	14.3 ± 5.7	5.9 ± 1.7
Spleen	6.5 ± 1.0	4.2 ± 0.5	4.1 ± 0.4	4.9 ± 1.3	2.7 ± 0.5
Kidney	5.0 ± 0.6	4.2 ± 0.5	4.1 ± 0.4	6.5 ± 1.5	7.0 ± 1.7
Liver	4.9 ± 0.5	5.0 ± 1.2	7.4 ± 2.4	4.9 ± 1.3	4.8 ± 1.3
Small intestine	2.6 ± 0.6	2.4 ± 0.8	2.0 ± 0.5	3.7 ± 1.2	1.6 ± 0.5
Salivary gland	3.7 ± 0.4	2.9 ± 0.2	2.9 ± 0.4	4.5 ± 1.0	2.7 ± 0.5
Adrenal gland	4.1 ± 1.3	4.0 ± 0.9	3.8 ± 0.5	6.0 ± 1.8	3.1 ± 0.7